

Dual communities in spatial networks

Received: 26 January 2022

Accepted: 10 November 2022

Published online: 03 December 2022

**Franz Kaiser**^{1,2}, **Philipp C. Böttcher**¹, **Henrik Ronellenfitsch**^{3,4},
Vito Latora^{5,6,7} & **Dirk Witthaut**^{1,2} 

Both human-made and natural supply systems, such as power grids and leaf venation networks, are built to operate reliably under changing external conditions. Many of these spatial networks exhibit community structures. Here, we show that a relatively strong connectivity between the parts of a network can be used to define a different class of communities: dual communities. We demonstrate that traditional and dual communities emerge naturally as two different phases of optimized network structures that are shaped by fluctuations and that they both suppress failure spreading, which underlines their importance in understanding the shape of real-world supply networks.

Community structures are a fundamental trait of complex networks and have found numerous applications in systems ranging from social networks¹ to biological networks^{2,3} and critical infrastructures such as power grids⁴. Typically, communities are defined by a strong connectivity within the community compared to a relatively weak connectivity between different communities^{1,5,6}. They may correspond to functional units of the network, for instance in metabolic networks⁷, or actual communities in social networks.

Intuitively, community structures play an important role for the spreading of failures or perturbations in networked systems. The low connectivity impedes spreading processes, such that perturbations can be expected to stay within the community, which is both predicted by theory^{8,9} as well as observed in experiments¹⁰. Community structures thus provide robustness in complex networks, but other structural patterns may have a comparable effect. In particular, it has been shown that hierarchical structures may provide similar features, for instance in vascular networks of plants^{11,12}.

In this article, we provide a unified view on the role of communities and hierarchies for network robustness based on the concept of graph duality. The dual graph is most naturally defined for spatially embedded networks, i.e., networks that are embedded in the plane without edges crossing each other. This class of networks includes a large variety of man-made and biological systems^{13–16}. The vertices of the dual correspond to the faces of the original, primal graph. Two dual vertices (faces) are

connected if they share at least one edge. Graph duality has been previously used to study fixed points in oscillator networks^{17,18} and to speed up network algorithms^{19,20}. Here we use this concept to reveal patterns in the network structure that are hidden in the primal graph. In particular, we establish dual communities—communities that are defined within the dual graph—and highlight their relation to hierarchical network structures. Furthermore, graph duality readily explains why both weak and strong connections can make a network robust: strong connections in the primal translate into weak connections in the dual and vice versa.

The article is organized as follows. We first demonstrate how different structural patterns impede spreading processes and thus contribute to the robustness of a network. Focusing on flow networks, we formalize the concept of graph duality and establish dual communities. Second, we investigate essential properties of dual communities, in particular their link to hierarchical patterns and the geometry of the community boundaries. Finally, we study the emergence and impacts of communities structures. Using optimization models, we study why networks develop a primal or a dual community structure. We provide a deeper analysis of the link between communities and network robustness by employing different simulation models. Throughout the article we use the terms graph and network interchangeably. The term “graph” stresses the structural aspects while “network” stresses the functional aspects of the system.

¹Forschungszentrum Jülich, Institute for Energy and Climate Research (IEK-STE), 52428 Jülich, Germany. ²Institute for Theoretical Physics, University of Cologne, 50937 Köln, Germany. ³Physics Department, Williams College, 33 Lab Campus Drive, Williamstown, MA 01267, USA. ⁴Department of Mathematics, Massachusetts Institute of Technology, Cambridge, MA 02139, USA. ⁵School of Mathematical Sciences, Queen Mary University of London, London E1 4NS, UK. ⁶Dipartimento di Fisica ed Astronomia, Università di Catania and INFN, 95123 Catania, Italy. ⁷Complexity Science Hub Vienna, 1080 Vienna, Austria.

✉ e-mail: d.witthaut@fz-juelich.de

Results

Network robustness and community structure

We first highlight how network robustness is related to the presence of communities for selected examples. Robustness is essential for critical infrastructures such as electric power grids. The high-voltage transmission grid of Scandinavia (Fig. 1a, c) has an obvious community structure due to geographic reasons. Finland is only weakly connected to the rest of Scandinavia through two high-voltage transmission lines. We simulate the impact of a transmission line failure, which is the biggest threat for large-scale blackouts²¹. We use the linear power flow or DC approximation^{22,23}, which will be described in detail below. The flow changes after the failure generally decay with the distance to the failing transmission line, but we also observe a strong impact of the community boundary. Flow changes are strongest in the community where the failure occurs, in this case Sweden. They are substantially suppressed in the other community, i.e., Finland, which also reduces the risk of a global cascade of failures.

Remarkably, a similar suppression of failure spreading is realized by strong connections. We consider the venation network of a leaf, which includes a strong central vein separating the left and right half (Fig. 1b, d). The flow of water and nutrients is described by a linear flow network¹¹, which is mathematically equivalent to the linear power flow approximation. If a secondary vein fails, we observe a very similar picture as for the power grid: flow changes generally decay and are strongly suppressed in the other half of the leaf. The central vein itself features large flow changes and thus provides a buffer function. We conclude that weak and strong connections can equally suppress the spreading of failures. We will show that both effects are fully equivalent and that they can be understood in terms of network communities, provided we generalize the definition of communities.

Before we move to a more detailed analysis, we demonstrate the generality of the observed phenomena. We consider a classic model

of network cascades^{24,25}. Nodes are either healthy/operational (state 0) or infected/faulty (state 1). A node i gets infected or faulty if the weighted average over all neighbors' states exceeds a certain threshold ϕ_i . Starting from a small amount of nodes in state 1, a cascade may emerge depending on the values ϕ_i and the structure of the network. As before, we consider networks which can be separated into two parts by either weak or strong connections (Fig. 1e, f). More precisely, we consider a lattice where the edges in the middle region have a tunable weight w , while all other edges have weight one (see “Methods” for details). We observe that a homogeneous network ($w = 1$) always leads to a global cascade, where all nodes are infected or faulty in the final state. A boundary, either by weak ($w \ll 1$) or strong ($w \gg 1$) connections, effectively stops the cascade. Only those nodes are infected, which are located in the same half as the initially infected ones.

Flow networks and dual communities

We have shown that strong connections can divide a network and enhance its robustness similarly as weak connections do. Even more, we can establish a full mathematical equivalence of weak and strong connections in the case of flow networks. This equivalence leads to a generalization of the definition of community structures in complex networks.

Linear flow networks arise in a variety of applications, including electric circuits^{26,27}, power grids^{22,23}, hydraulic networks^{28,29}, and vascular networks of plants¹¹. In these networks, the flow from node i to node j is given by $F_{i \rightarrow j} = w_{ij} \cdot (\theta_i - \theta_j)$, where w_{ij} is the connectivity or conductivity of the edge (i, j) . The nodal variable θ_i describes the local voltage or potential in an electric circuit, the voltage phase angle in a power grid, or the pressure in a hydraulic or vascular network. The flows have to satisfy the continuity equation (or Kirchhoff's current law, KCL) at every node i of the network, $\sum_j F_{i \rightarrow j} = P_i$, where P_i is the inflow to the network.

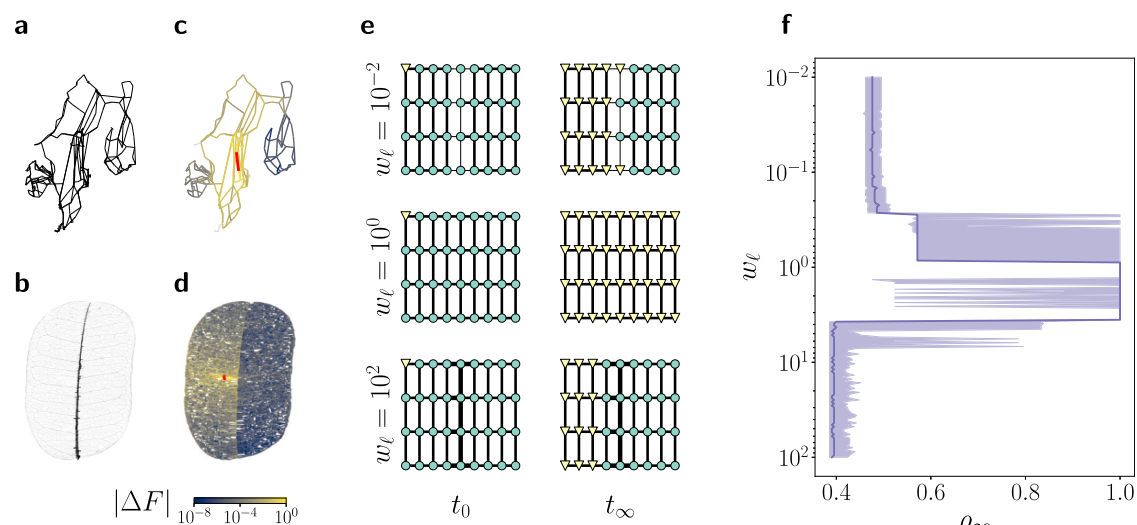


Fig. 1 | Different structural patterns separate networks and increase network robustness. **a** Topology of the Scandinavian power grid, with weak connectivity between different geographic units, in particular Finland. **b** Venation network of the leaf *Schizolobium amazonicum*, with a strong central vein separating the leaf into left and right. The width of the lines in **a**, **b** encode the edge weights. **c**, **d** Flow changes $|\Delta F|$ after the failure of a single edge (colored in red) for the two networks shown in **a**, **b**. The impact of the failure is strongly suppressed in another part of the network, i.e., in Finland and the right half of the leaf, respectively. This highlights the existence and impact of boundaries that separate the network into communities. **e** Simulation of a classic model of global cascades^{24,25} in a lattice with inhomogeneous edge weights. Edges in the middle have weight w_ℓ (indicated by thin/

thick lines), while all other edges have a weight of $w_{ij} = 1$ (see “Methods” for details). Infected/faulty nodes are shown as yellow triangles, healthy/operational nodes as green circles. A global cascade occurs for a homogeneous lattice ($w_\ell = 1$), while both weak ($w_\ell = 10^{-2}$) and strong connections ($w_\ell = 10^2$) stop the cascade from propagating to the right part of the network. **f** Final fraction ρ_∞ of nodes that become infected/faulty during the cascade as a function of the weight parameter w . The line represents the median and the shaded region the 25–75% quantile for 1000 random initial conditions. For homogeneous lattices ($w = 1$), the cascade reaches all nodes ($\rho_\infty = 1$). For both weak ($w \ll 1$) and strong ($w \gg 1$) conditions, the cascade stops at the boundary such that $\rho_\infty \approx 0.5$.

These equations can be recast in a compact matrix notation. Let N denote the number of nodes and M the number of edges in the network, which we assume to be connected. We fix an orientation for each edge to keep track of the direction of flows and define the edge-node incidence matrix $\mathbf{I} \in \mathbb{R}^{M \times N}$ as

$$I_{\ell n} = \begin{cases} +1 & \text{if edge } \ell \text{ starts at node } n, \\ -1 & \text{if edge } \ell \text{ ends at node } n, \\ 0 & \text{otherwise.} \end{cases} \quad (1)$$

The edge weights are summarized in a diagonal matrix $\mathbf{W} = \text{diag}(w_1, \dots, w_M)$ while all other quantities are summarized in vectors $\boldsymbol{\theta} = (\theta_1, \dots, \theta_N)^\top$, $\mathbf{P} = (P_1, \dots, P_N)^\top$, $\mathbf{F} = (F_1, \dots, F_M)^\top$. Note, the ordering of the edges in the edge-node incidence matrix \mathbf{I} and the weights in the diagonal matrix \mathbf{W} have to be consistent such that the weight of edge k connecting nodes i and j is given by $w_k = w_{ij}$. Then the relation of flows and potentials is given by $\mathbf{F} = \mathbf{W}\mathbf{I}\boldsymbol{\theta}$ and Kirchhoff's current law reads

$$\mathbf{P} = \mathbf{I}^\top \mathbf{F} = \underbrace{\mathbf{I}^\top \mathbf{W} \mathbf{I}}_{=: \mathbf{L}} \boldsymbol{\theta}. \quad (2)$$

Equation (2) is a discrete Poisson equation that determines the potential $\boldsymbol{\theta}$ up to an irrelevant additive constant. The matrix $\mathbf{L} \in \mathbb{R}^{N \times N}$ is nothing but the well known graph Laplacian with components

$$L_{ij} = \begin{cases} -w_{ij} & \text{if } i \text{ is connected to } j, \\ \sum_k w_{ik} & \text{if } i = j, \\ 0 & \text{otherwise.} \end{cases} \quad (3)$$

The Laplacian is a central object in spectral graph bisection³⁰, a classic method of community detection, which will be further elaborated below.

The above description focuses on the nodes of the network, with the nodal potentials $\boldsymbol{\theta}$ being the central quantity of interest. An equivalent description exists that focuses on the edges of the network and the flows \mathbf{F} . The starting point is the KCL $\mathbf{I}^\top \mathbf{F} = \mathbf{P}$. This linear set of equations is underdetermined in terms of \mathbf{F} , such that the general solution can be written as the sum of a particular solution and an arbitrary solution of the associated homogeneous equation, namely

$$\mathbf{F} = \mathbf{F}_{\text{part}} + \mathbf{F}_{\text{hom}}. \quad (4)$$

The vector \mathbf{F}_{hom} describes a flow without sources or sinks, that is, a collection of cycle flows. The cycle flows form a vector space (the cycle space) such that we can expand each cycle flow into a suitable basis. A distinguished basis exists for plane graphs, i.e., graphs embedded in the plane, which can be constructed in the following way. A face of a plane graph is a region that is bounded by edges, but contains no edges in the interior. The boundary edges of each face then provide one basis vector of the cycle space. Further details are given in the Supplementary Information.

To keep track of the basis, we introduce the cycle edge incidence matrix $\mathbf{C} \in \mathbb{R}^{M \times (M-N+1)}$ with components

$$C_{\ell c} = \begin{cases} +1 & \text{if edge } \ell \text{ is part of face } c, \\ -1 & \text{if reversed edge } \ell \text{ is part of face } c, \\ 0 & \text{otherwise.} \end{cases} \quad (5)$$

Then we can write the general solution of the KCL as

$$\mathbf{F} = \mathbf{F}_{\text{part}} + \mathbf{C} \mathbf{f} \quad (6)$$

with an arbitrary cycle flow vector \mathbf{f} . The actual values of the cycle flows are then determined by Kirchhoff's voltage law (KVL), which states that the potential differences around any closed cycle sum up to zero. In fact it is sufficient to enforce this for the $M - N + 1$ basis cycles. We can thus formulate the KVL in terms of the flow vector \mathbf{F} as

$$\mathbf{C}^\top \mathbf{W}^{-1} \mathbf{F} = \mathbf{0}. \quad (7)$$

Crucially, this equation includes the matrix \mathbf{W}^{-1} which translates flows into potential differences. Substituting Eq. (6) then yields

$$\mathbf{Q} = \underbrace{\mathbf{C}^\top \mathbf{W}^{-1} \mathbf{C}}_{=: \mathbf{L}^*} \mathbf{f}. \quad (8)$$

Notably, this equation has the same mathematical structure as Eq. (2): It is a discrete Poisson equation with a Laplacian matrix \mathbf{L}^* and a source term $\mathbf{Q} = -\mathbf{C}^\top \mathbf{W}^{-1} \mathbf{F}_{\text{part}}$. However, the Laplacian \mathbf{L}^* is not defined on the original primal graph, but on the dual graph. The vertices of this dual graph are given by the faces of the primal graph, while two nodes of the dual graph are connected by a dual edge if the corresponding faces share an edge.

Comparing the Laplacian of the primal graph $\mathbf{L} = \mathbf{I}^\top \mathbf{W} \mathbf{I}$ to that of the dual graph $\mathbf{L}^* = \mathbf{C}^\top \mathbf{W}^{-1} \mathbf{C}$, we see another essential aspect of graph duality: The weights of the dual edges are inverse to the weights of the primal edges. More precisely, we find the dual weights

$$w_{c,d}^* = \sum_{\ell \in c,d} \frac{1}{w_\ell} \quad (9)$$

of the edge that connects the nodes c and d in the dual graph corresponding to faces c and d that share the edge ℓ in the primal graph. This relation shows most clearly why weak and strong connections can both affect the robustness and the community structure of a network. Strong connections in the primal correspond to weak connections in the dual and vice versa. Similarly, a strong central vein in the primal corresponds to weak connections in the dual and thus to a pronounced community structure.

We have now introduced all mathematical tools to identify dual communities in planar complex networks. Starting from the primal network, we identify all faces and define the dual graph with weights given by Eq. (9). Then dual communities can be extracted by means of any standard community detection algorithm.

In the following, we focus on spectral graph bisection because of its direct link to the graph Laplacian—which is the central object in the above analysis. This method relies on the fact that the community structure is encoded in the second smallest eigenvalue of the graph Laplacian $\lambda_2 \geq 0$, known as the algebraic connectivity or Fiedler value, which vanishes if the graph consists of two disconnected components and increases with increasing connectivity between the communities. The graph nodes are then assigned to one of two communities based on the corresponding eigenvector \mathbf{v}_2 , the Fiedler vector: two vertices j and i are in the same community if they share the same sign of the Fiedler vector⁵.

$$\text{sign}((\mathbf{v}_2)_i - h) = \text{sign}((\mathbf{v}_2)_j - h), \quad (10)$$

where $h \in \mathbb{R}$ is a threshold parameter. Here, we choose $h = 0$.

This method can be straightforwardly applied to the dual graph, replacing the primal Laplacian \mathbf{L} by its dual counterpart \mathbf{L}^* . The algebraic connectivity of the dual is measured by the second eigenvalue λ_2^* and the associated eigenvector is used to identify the dual communities. We find that dual communities appear naturally in real-world networks such as the venation networks of leaves (Fig. 2b, e). In the following, we discuss essential properties of dual communities, in

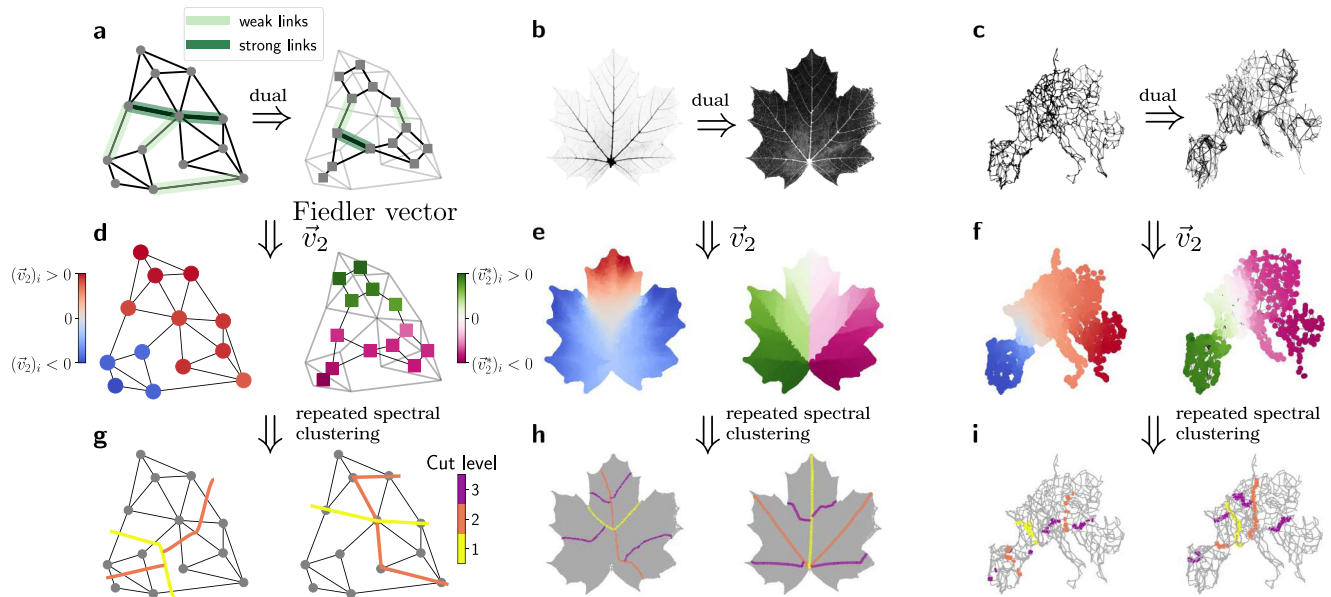


Fig. 2 | Primal and dual communities and hierarchies in spatial networks. **a** A plane graph with edges characterized by either large (dark green), small (light green) or intermediate edge weights, and its associated dual graph. The dual graph is constructed by transforming each face of the graph into a node of the dual, and adding dual edges whenever two faces share an edge. Notice that an edge with large weight shared by two faces will imply a weak link between the two corresponding nodes in the dual graph (see Eq. (9)). **d** Spectral clustering by means of the Fiedler vector \vec{v}_2 reveals the community structure in both the graph (left) and its dual (right). **g** Based on repeated spectral clustering, the graphs are further decomposed into a hierarchy of smaller sub-units which is different in the graph (left) and its

(dual). **b, e, h** If we perform the same analysis on the venation network of a leaf of *Acer platanoides*, a decomposition of the original graph does not provide useful information (**e, h**, left). A decomposition of the dual graph, however, reveals the hierarchical organization and the functional units of the venation network (**e, h**, right). **c, f, i** Applying the same procedure to the Central European power grid, (**i**, left) and its dual (**i**, right) show that primal and dual hierarchies provide different, but equally useful information about the network structure. We may conclude that this network represents an intermediate case between primal and dual community structure (see main text for details).

particular their relation to hierarchical structures, and provide a thorough analysis of the dual algebraic connectivity λ_2^* . We stress that other community detection methods can be applied to the dual graph equally well and yield comparable results (cf. Supplementary Fig. S6).

Dual communities reveal hierarchical organization of supply networks

The spectral clustering method for community detection can be applied to both the primal and the dual graph, revealing different structural information about the network (Fig. 2). Furthermore, we can use this approach to extract a network's hierarchical organization as follows. Starting from the initial network, we compute the Fiedler vector, identify the communities and then split the network into two parts at the resulting boundary by removing all edges between the communities. Then we iterate the procedure starting from the subgraphs obtained in the previous step. Repeated application of this procedure reveals different boundaries and thus different hierarchies in the primal graph and in its dual (Fig. 2g, see “Methods” for details).

Leaf venation networks are archetypal examples of hierarchically organized networks, with a thick primary vein in the middle and medium secondary veins that supply thin subordinated veins (Fig. 2b). The thick veins separate the network into distinct parts—for instance, the left and right half separated by the primary vein. This characteristic organization is clearly revealed by dual community detection. Spectral graph bisection identifies the primary vein that separates the left and the right half of the leaf. Repeating the bisection then shows that this organizational pattern repeats in a hierarchical order: dual communities are split by secondary veins in a repeated manner (Fig. 2h). Remarkably, an analog decomposition in the original

primal graph does not provide any useful information on the network organization.

We conclude that leaf venation networks clearly display a dual community structure, where the boundary of the dual communities coincide with the primary and secondary veins. Hence, dual community detection allows to identify hierarchical organization patterns in complex networks. We will provide a more formal treatment of the relation between strong veins and dual communities below.

As a second example, we now turn to another type of spatially embedded supply networks: power grids. Figure 2c shows the European power transmission grid and its dual graph. Again, a hierarchical decomposition reveals different levels of hierarchies in the grid that correspond to its functional components. These components may also be interpreted geographically: the mountain ranges such as the Pyrenees or the Alps as well as the former Iron Curtain are clearly visible in the decomposition of the primal graph. Remarkably, both primal and dual decompositions provide useful structural information here. In particular, there is a dual community boundary at cut level three that spans Hungary and the border region between Slovenia and Croatia and closely corresponds to a weak spot in the European power system, where the grid was split into two mutually asynchronous fragments on January 8, 2021³¹. Another split occurred on the 24th of July between Spain and France—where both the primal and the dual decomposition detect a community boundary³².

Although mathematically similar^{12,33,34}, the two types of networks we studied display different structural hierarchies and communities. Whereas leaf venation networks are evolutionarily optimized, the structure of power grids depends strongly on historical aspects and their ongoing transition to include a higher share of renewable energy sources. This transition aspect also manifests in their community structure, as we will see further below.

Connectivity and the geometry of community boundaries

The algebraic connectivity λ_2 of a graph is closely related to its topological connectivity—the amount of connectivity between the two communities³⁵. For a weighted graph, one can derive the upper bound (see Supplementary Note 2)

$$\lambda_2 \leq \mu_2 = \frac{N_1 + N_2}{N_1 N_2} \sum_{\ell \in S} w_\ell, \quad (11)$$

where N_1 and N_2 respectively count the number of nodes in the two communities. The set S contains all edges which are not within one of the two communities but in between, providing a weak connection of the communities (Fig. 3a). This set is referred to as a cut-set: If all edges in S are removed, the graph is cut into the two communities. Notably, the bound becomes exact in the limit of vanishing connectivity ($\mu_2 \rightarrow 0$) as shown in the Supplementary Information.

We derive an analogous bound for dual communities, transferring geometric concepts from the primal to the dual. In particular, we derive an analog to the cut-set S , which contains all edges, which are elements of neither of the two components. Consider a decomposition of the dual graph $G^* = (V^*, E^*)$, where the dual vertex set V^* is separated into two components V_1^* and V_2^* . Two faces $c \in V_1^*$ and $d \in V_2^*$ are connected in the dual, if they share at least one edge in the primal graph. Hence, we will find a set of primal edges which belong to both of the two components (Fig. 3b). These primal edges, together with their

terminal vertices, constitutes a path p in the primal graph. In the following, we will refer to p as a cut-path as its removal disconnects the graph. The edges along the cut-path essentially determine the community structure of the dual graph and its algebraic connectivity. Given a cut-path p , we find the bound

$$\lambda_2^* \leq \mu_2^* = \frac{N_1^* + N_2^*}{N_1^* N_2^*} \sum_{\ell \in p} \frac{1}{w_\ell}, \quad (12)$$

where $N_{1,2}^* = |V_{1,2}^*|$ counts the number of nodes in the dual communities. Notably, the expression μ_2^* does not only provide an upper bound for the algebraic connectivity λ_2^* , but an approximation that becomes exact in the limit of vanishing dual connectivity. We prove these statements rigorously in the Supplementary Information.

The relation of cut-paths and dual communities is further investigated in Fig. 4 for both synthetic networks and leaf venation networks. We first consider a square lattice with a tunable dual community structure: The edges in the central vein have a higher weight w_1 than the remaining edges w_0 . We find that the dual algebraic and topological connectivity λ_2^* and μ_2^* become virtually indistinguishable for $w_1/w_0 \geq 10^2$. In venation networks, the boundaries between the dual communities, i.e., the cut-paths, correspond to the primal and secondary veins as described above. A good agreement between μ_2^* and λ_2^* is found especially for the two smaller venation networks from the *Parkia* and *Schizolobium* family. This result further emphasizes the intimate relation of dual communities and hierarchical organization in complex networks.

Why do primal and dual communities emerge?

Understanding how the structure of optimal supply networks emerges is an important aspect of complex networks research^{11,36–38}. In cases where a single source supplies the entire network, it is well established that fluctuations in the supply can cause a transition from a tree-like topology to a structure with loops^{11,34,36}. We extend this result by studying how the increase in fluctuations influences the optimal network structure in supply networks with multiple strongly fluctuating sources and weakly fluctuating sinks. This design is highly relevant for many real-world applications, e.g., when considering a power grid that is based on decentralized renewable energy sources that fluctuate more than conventional carriers.

To interpolate between strongly fluctuating sources and weakly fluctuating ones, we first use a similar model as in ref. 36.

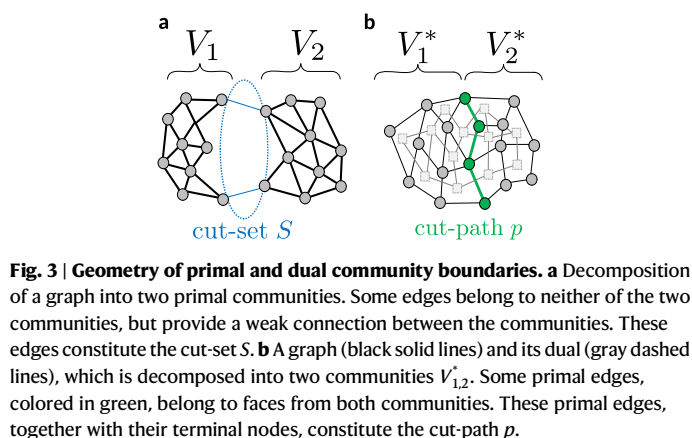


Fig. 3 | Geometry of primal and dual community boundaries. **a** Decomposition of a graph into two primal communities. Some edges belong to neither of the two communities, but provide a weak connection between the communities. These edges constitute the cut-set S . **b** A graph (black solid lines) and its dual (gray dashed lines), which is decomposed into two communities $V_{1,2}^*$. Some primal edges, colored in green, belong to faces from both communities. These primal edges, together with their terminal nodes, constitute the cut-path p .

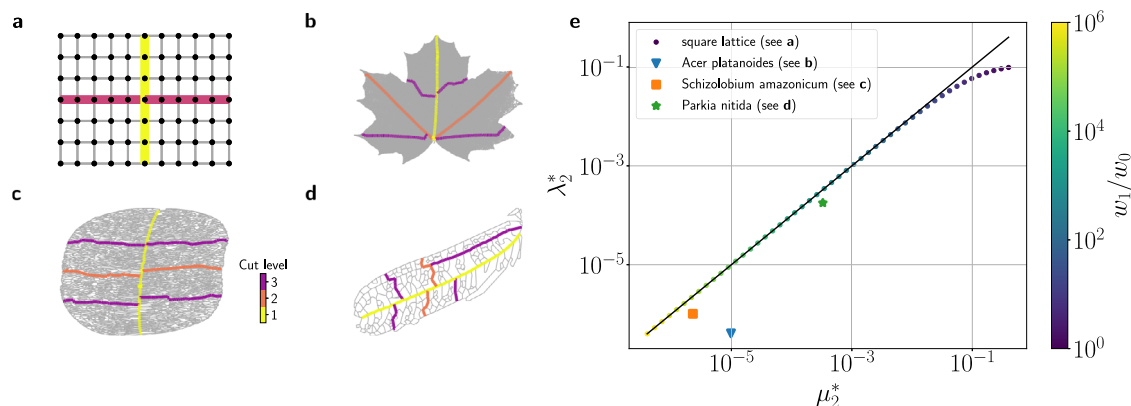


Fig. 4 | Algebraic and Topological Connectivity in the dual graph of synthetic and real-world networks. **a** A square lattice with a tunable dual community structure. The edge weights along the central vein w_1 are stronger than the weights w_0 of the remaining edges. The ratio w_1/w_0 can be tuned to test the relation of algebraic and topological connectivity given by Eq. (12). **b–d** Hierarchical organization in leaf venation networks of three different species revealed by repeated graph bisection of the dual graph. The dual

community boundary (yellow) constitutes a cut-path p . **e** Comparison of the dual algebraic connectivity λ_2^* and the dual topological connectivity μ_2^* defined in Eq. (12). Circles refer to the case of the square lattice with the color of the circles indicating the fraction w_1/w_0 . The topological connectivity μ_2^* provides a rigorous upper bound for λ_2^* , but also a good approximation for large parameter regions. This correspondence shows how dual communities are decomposed by a strong connectivity along the boundary.

We consider a linear flow network consisting of a triangular lattice with N nodes of which N_s are sources and $N - N_s$ are sinks whose outflows are fluctuating iid Gaussian random variables. Additionally, we add fluctuations only to the sources of the networks that can be tuned by the additional variance σ_D^2 (see “Methods”). We then compute the optimal structure and edge weights of the network that minimize the total dissipated energy $D = \sum_i \langle F_i^2 \rangle / w_i$ averaged over the fluctuating inflows and outflows. Resources for building the network are assumed to be limited, which translates into the constraint $\sum_e w_e \leq 1$. The cost parameter γ quantifies how expensive the increase of an edge weight is and was set to $\gamma = 0.9$ for the examples presented in this manuscript (see Supplementary Note 4 for more information). Results for $N_s = 2$ sources are shown in Fig. 5, and further results for $N_s = 3$ are provided in the Supplementary Information.

We find that the optimal network structure changes strongly as the fluctuations increase. For weak fluctuations, $\sigma_D^2 \approx 1$, each of the N_s sources supplies the surrounding area of the network. Only weak connections are established between the areas to cope with the small residual imbalances. Hence, the optimal networks show a pronounced primal community structure (see Fig. 5a).

For strong fluctuations, $\sigma_D^2 \gg 1$, a local area supply is no longer possible and long-distance connectivity is required. Remarkably, this

connectivity is established in one central vein that links the two fluctuating sources (see Fig. 5b). As a consequence, the optimal networks show a pronounced dual community structure similar to leaf venation networks. We can capture the transition from a primal to a dual community structure in terms of the primal and dual Fiedler values (Fig. 5e). Increasing σ_D^2 , we observe a smooth crossover from primal communities with $\lambda_2 \rightarrow 0$ to dual communities with $\lambda_2^* \rightarrow 0$. We note that a similar picture is found if the Fiedler values λ_2 and λ_2^* are replaced by another measure such as the modularity (see Supplementary Fig. S1). We conclude that optimal supply networks typically have a community structure—whether it is primal or dual depends on the degree of fluctuations.

Strikingly, an analogous transition is observed for actual power transmission grids when optimizing the network structure for different levels of fluctuating renewable energy sources. We consider the European power transmission grid and optimize its network structure for different carbon dioxide (CO₂) emission reduction targets compared to the year 1990 ranging from 60% to 100% reduction using the open energy system model “PyPSA-Eur”³⁹ (see “Methods” for details). In Supplementary Figs. S3 and S4, we illustrate how the generation mix in the optimized power system changes for different emission scenarios from conventionally dominated grids to highly renewable grids.

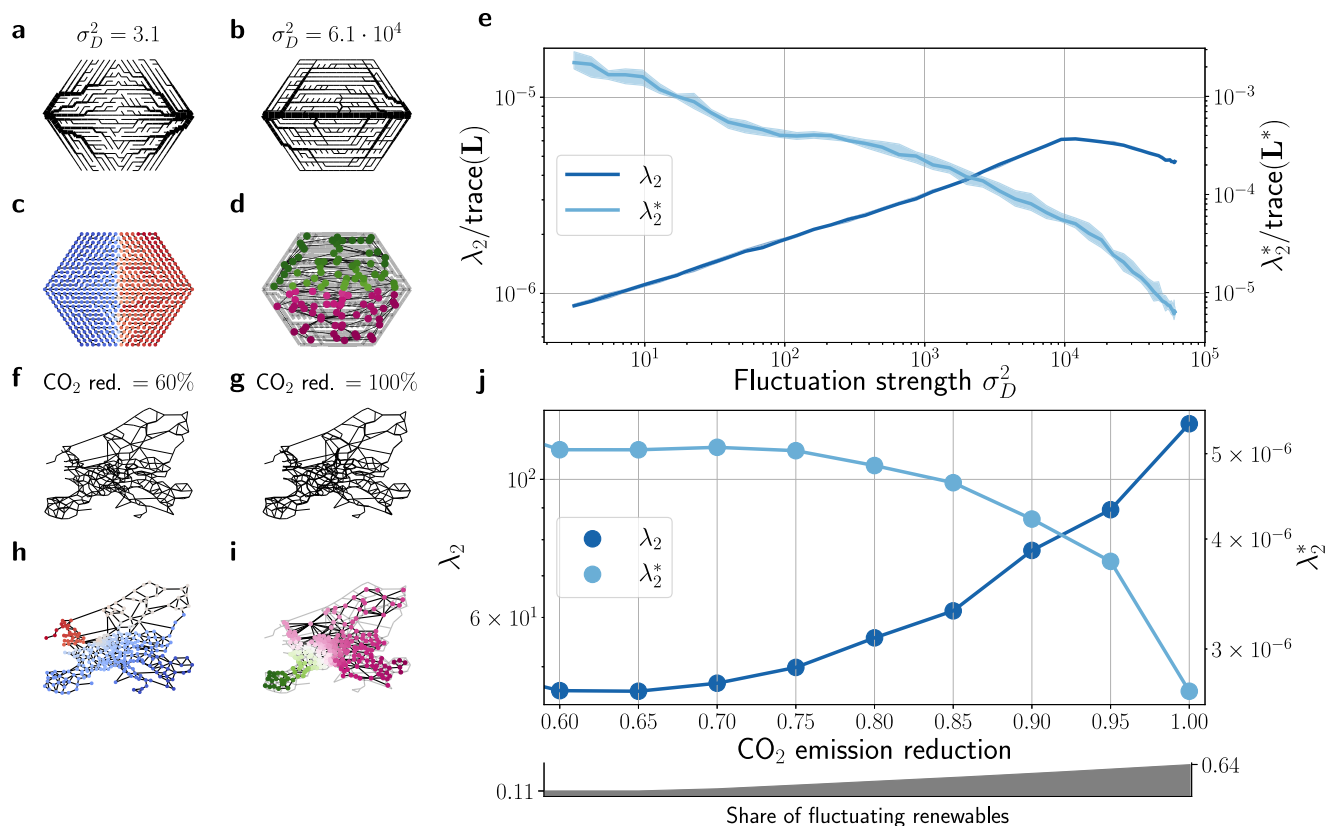


Fig. 5 | Primal and dual communities emerge naturally in optimal supply networks. **a, b** We consider a triangular lattice with two fluctuating sources located at the leftmost and the rightmost node and Gaussian sinks attached to all other nodes. The strength of the two sources fluctuates following a Dirichlet distribution with variance σ_D^2 (see “Methods”). For each value of σ_D^2 , we find the network structure and the edge weights that minimize the total dissipated energy D assuming limited resources. **c, d** The optimal network structure shows a transition from primal to dual communities measured by the Fiedler vectors (color code) of the primal graph (**c**) or dual graph (**d**). **e** The scaling of the corresponding primal (λ_2 , dark blue) and dual (λ_2^* , light blue) Fiedler value confirms the transition. The shaded regions indicate the 25–75% quantiles for different runs. **f, g** A transition from primal to dual

community structure is also observed in optimization models of the European power grid when generation shifts to fluctuating renewables. The figure shows the optimal network structures and transmission line capacities in a cost optimal system for different carbon-dioxide (CO₂) emission reduction levels. **h, i** Primal and dual communities are identified by the Fiedler vectors (color code) of the primal or dual graph. **j** The transition is confirmed by the scaling of primal and dual Fiedler values for increasing emission reduction which corresponds to an increasing share of fluctuating renewables (lower axis). Simulations were performed with the high-resolution European energy system model “PyPSA-EUR”³⁹ that optimizes the investments and operations of generation and transmission infrastructures for minimum system costs.

We find that the decarbonization of power generation drives a transition from primal to dual communities in the grid. A reduction in generation-based CO₂ emissions corresponds to an increased share of power being produced by fluctuating renewable energy sources. With increasing penetration of fluctuating renewables, we observe a decrease in the dual Fiedler value λ_2^* and an increase in the primal Fiedler value λ_2 , which indicates a transition from primal to dual communities in the optimized networks (Fig. 5j). Hence, the primal-dual transition emerges both in fundamental models and in realistic high-resolutions simulations of spatial networks.

How do primal and dual communities determine network robustness?

Primal and dual communities both impede the spreading of failures and thus improve the robustness of complex networks as shown in Fig. 1. We will now provide a more detailed and quantitative analysis of this connection for two important systems: flow networks and coupled oscillator networks.

We first consider linear flow networks using the theoretical framework introduced above. Robustness is quantified by a sensitivity factor, measuring the response of the network flows \mathbf{F} to a perturbation. As a perturbation, we add an inflow ΔP at a node v_1 and an outflow of the same amount at another node v_2 . Here, we focus on the case where v_1 and v_2 are the two end nodes of an edge $e = (v_1, v_2)$ and treat the general case in the Supplementary Information. The source vector in the Poisson Eq. (2) then changes as

$$\mathbf{P} \rightarrow \mathbf{P}' = \mathbf{P} + \Delta P \mathbf{I}_e^\top \mathbf{I}_e \quad (13)$$

and $\mathbf{I}_e \in \mathbb{Z}^M$ is the indicator function for edge e , which is equal to one at the positions indicated by the subscript and zero otherwise. Inverting the discrete Poisson Eq. (2), we then find that the network flows change by the amount

$$\Delta \mathbf{F} = \Delta P \mathbf{W} \mathbf{L}^\dagger \mathbf{I}_e^\top \mathbf{I}_e, \quad (14)$$

where \mathbf{L}^\dagger is the Moore–Penrose pseudoinverse of the primal graph Laplacian. We then define a sensitivity factor as the ratio of the flow

change at edge ℓ and the perturbation strength ΔP as^{40,41}

$$\eta_{v_1, v_2, \ell} = \frac{\Delta F_\ell}{\Delta P} = w_\ell \mathbf{I}_\ell^\top \mathbf{L}^\dagger \mathbf{I}_e. \quad (15)$$

We note that the sensitivity factor is widely used in the context of power system security analysis, where it is referred to as a power transfer distribution factor^{40,41}. Importantly, the sensitivity factor may also be used to simulate the failure of an edge $e = (v_1, v_2)$ by choosing the inflow ΔP accordingly (see Supplementary Information).

The sensitivity factor $\eta_{v_1, v_2, \ell}$ elucidates the relation between primal communities and network robustness⁸. In the Supplementary Information, we treat the limiting case of vanishing connectivity between the communities and show the following: If the edges e and ℓ are in different communities, η vanishes in the same way as the Fiedler value λ_2 . If the edges e and ℓ are in the same community, η remains finite as $\lambda_2 \rightarrow 0$.

Remarkably, we can find an analogous description in the dual graph^{19,20}. In Eq. (4), we choose the particular solution as $\Delta F_{\text{part}} = \Delta P \mathbf{I}_e$. We can then compute the cycle flows \mathbf{f} from Eq. (8) and substitute the result into Eq. (6) to obtain the change of network flows^{19,20}

$$\Delta \mathbf{F} = -\Delta P \mathbf{C}(\mathbf{L}^*)^\dagger \mathbf{C}^\top \mathbf{W}^{-1} \mathbf{I}_e + \Delta P \mathbf{I}_e. \quad (16)$$

The sensitivity factor for all edges $\ell \neq e$ thus reads

$$\eta_{v_1, v_2, \ell} = -\frac{1}{w_e} \mathbf{I}_\ell^\top \mathbf{C}(\mathbf{L}^*)^\dagger \mathbf{C}^\top \mathbf{I}_e. \quad (17)$$

We see that the dual Laplacian \mathbf{L}^* contributes to the sensitivity factor $\eta_{v_1, v_2, \ell}$ in exactly the same way as the primal Laplacian \mathbf{L} in Eq. (15). Hence, we conclude that primal and dual community structures determine network flows in an equivalent manner. If the edges e and ℓ are in different dual communities, η will vanish proportional to the dual Fiedler value λ_2^* . If the edges e and ℓ are in the same community, η remains finite in the limit $\lambda_2^* \rightarrow 0$.

We now quantify this effect. To analyze the impact of a community structure, we consider a square lattice with tunable edge weights.

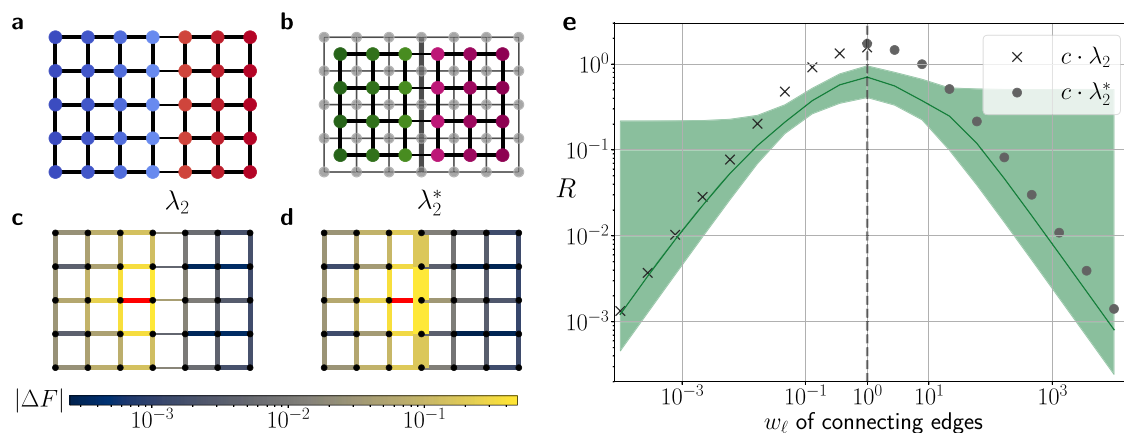


Fig. 6 | Primal and dual communities inhibit failure spreading. **a, b** A square grid is divided into **a** two primal communities by weakening the central horizontal edges or **b** into two dual communities by strengthening the central vertical edges. The Fiedler vector (color code) reveals the community structure. **c, d** Both primal and dual communities inhibit flow changes $|\Delta F|$ (color coded) in the other community after the failure of a single edge (red) with unit flow in a given community. **e** We interpolate between primal and dual communities in a square grid of size 21×10 by

tuning the weight w_e of the horizontal edges or vertical edges (see **a, b**). The flow ratio R reveals that failure spreading to the other community is largest for $w_e = 1$. It decays for either type of community as measured by primal and dual Fiedler values λ_2 (crosses) and λ_2^* (circles), respectively. The green line represents the median value and the shaded regions indicate the 25% and 75% quantiles. The symbol c denotes a normalization constant used to improve comparison with R .

We either reduce the edge weights w_ℓ across the boundary, i.e., in the cut-set, to induce a primal community structure, or we increase the edge weights w_ℓ along the boundary, i.e., in the cut-path, to induce a dual community structure (Fig. 6a, b). We then consider an inflow and simultaneous outflow ΔP at two nodes v_1 and v_2 , respectively, that are connected via an edge $e = (v_1, v_2)$. We then compare the resulting flow changes in the same (S) and the other (O) community as the given edge e . To this end, we evaluate the ratio of flow changes $R(e, d)$ in the two communities at a given distance d to the trigger edge e ³³

$$R(e, d) = \frac{\langle |\Delta F_k| \rangle_d^{k \in O}}{\langle |\Delta F_r| \rangle_d^{r \in S}} = \frac{\langle |\eta_{v_1, v_2, k}| \rangle_d^{k \in O}}{\langle |\eta_{v_1, v_2, r}| \rangle_d^{r \in S}}. \quad (18)$$

Here, $\langle \cdot \rangle_d^{\ell \in C}$ denotes the average over all edges ℓ in a community C at a given distance d to the trigger edge e . To be able to neglect the effect of a specific edge and the distance, we average over all possible trigger edges e and distances d to arrive at the mean flow ratio

$$R = \langle R(e, d) \rangle_{e, d}. \quad (19)$$

The mean flow ratio ranges from $R \approx 0$ if the other module is weakly affected, i.e., there is a strong community effect, to $R \approx 1$ if there is no noticeable effect. We note that R describes flow changes after perturbations in the inflows and outflows as well as flow changes as a result of the complete failure of edges (see Supplementary Information).

Figure 6 illustrates that both primal and dual communities suppress flow changes in the other community. The mean flow ratio R decays for either community structure. In particular, this decay is well-captured by the Fiedler value of the primal (λ_2) and the dual (λ_2^*) graph.

These findings are not restricted to linear flow networks, but hold for all diffusively coupled networked systems. We illustrate this effect

for a network of second-order phase oscillators that arises in the analysis of electric power grids^{18,42} or mechanically coupled systems⁴³ and as a generalization of the celebrated Kuramoto model⁴⁴. The phase $\vartheta_i(t)$ of each oscillator $i = 1, \dots, N$ evolves according to

$$M_i \ddot{\vartheta}_i + D_i \dot{\vartheta}_i = \omega_i + \sum_{j=1}^N w_{ij} \sin(\vartheta_j - \vartheta_i), \quad (20)$$

where M_i is the inertia and D_i the damping of the i th oscillator. To analyze the impact of community structures, we consider a honeycomb lattice with tunable edge weights, with either low weights $w_{ij} \leq 1$ across the boundary or high weights $w_{ij} \geq 1$ along the boundary. The weights of all remaining edges are set to $w_{ij} = 1$ and $w_{ij} = 0$ if no edge exists between nodes i and j .

We now investigate how the steady states of such a network react to a localized perturbation near the community boundary (Fig. 7a, b). The oscillators relax to a phase-locked state after a short transient period, but the steady-state phases are shifted by an amount $\Delta\vartheta_i$. We recall that a global phase shift is physically irrelevant and is henceforth discarded. The response $|\Delta\vartheta_i|$ crucially depends on the location of the oscillator—being strongly suppressed across the community boundary (Fig. 7a–d). To evaluate the impact of the network structure, we quantify the overall network response by the variance of the phases within a community C ,

$$\text{var}(|\Delta\vartheta_i|_C) = \sum_{i \in C} |\Delta\vartheta_i|^2 - \left(\sum_{i \in C} |\Delta\vartheta_i| \right)^2. \quad (21)$$

This overall response is generally suppressed in the non-perturbed community, for primal as well as for dual communities. The more pronounced the community structure, the stronger the suppression of the response (Fig. 7e). We note that for the current example some differences exist between primal and dual communities.

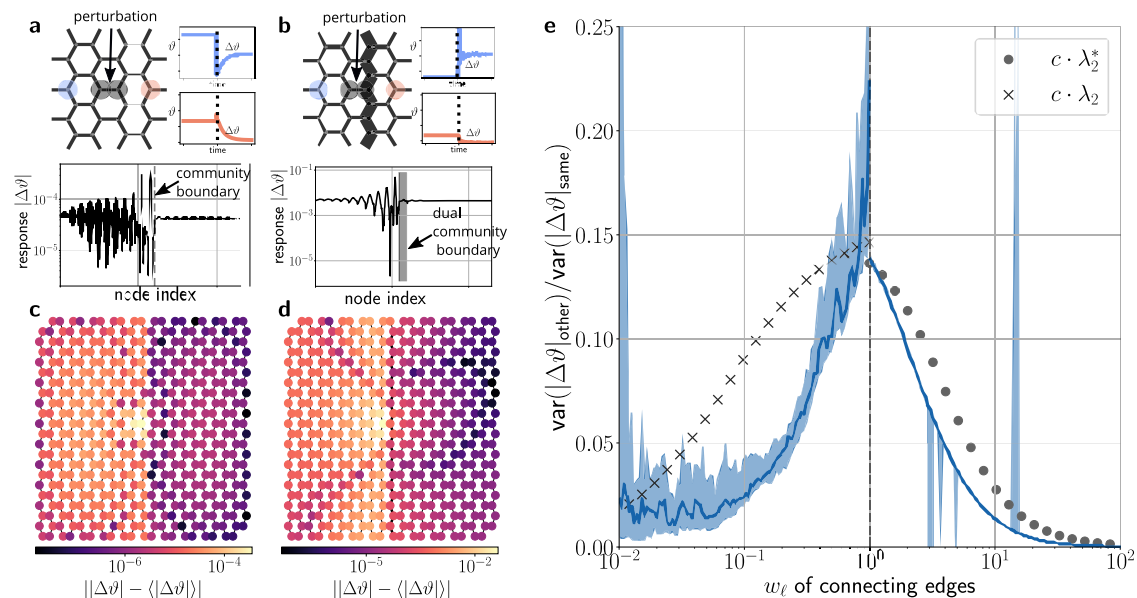


Fig. 7 | Suppression of failure spreading in oscillator networks. **a, b** We analyze the response of a network of phase oscillators (Eq. (20)) to a localized perturbation. We consider a honeycomb lattice with **a** a primal community structure induced by weak connectivity across the community boundary and **b** a dual community structure induced by strong connectivity along the boundary. After the perturbation the oscillators relax back to a phase-locked state with phases shifted by $\Delta\vartheta_i$. **c, d** We find that the response $|\Delta\vartheta_i|$ is strongly suppressed in the non-perturbed community. **e** The overall network response is quantified by the variance of the

response within a network community (Eq. (21)). The response in the non-perturbed community is strongly suppressed—the more pronounced the community structure, the stronger the attenuation. The existence of a primal or dual community structure is indicated by primal and dual Fiedler values λ_2 (crosses) and λ_2^* (circles), respectively. The blue line represents the median value and the shaded regions indicate the 25 and 75 percentiles for different random realizations of the natural frequencies ω_i . The symbol c denotes a normalization constant used to improve comparison with the response.

In particular, statistic fluctuations are larger in the case of primal communities.

We conclude that the impact of community boundaries, both primal and dual, extends to all diffusively coupled networked systems. Our finding can be further substantiated by a linear response analysis⁸, which highlights the structural similarity to linear flow networks. Furthermore, we note that related phenomena were observed for models of information diffusion in networks of different modularity²⁵. This finding is closely related, as the diffusion model includes an averaging over all adjacent nodes in the network.

Discussion

We have introduced a way to define and identify dual communities in planar graphs. We demonstrated that both primal and dual community structures emerge as different phases of optimized networks – whether the one or the other is realized in a given optimal network depends on the degree of fluctuations. In addition to that, both types of communities have the ability to suppress failure spreading. They are thus optimized to limit the effect of edge failures or other perturbations.

An important difference between primal and dual communities is the fact that the former are based on a weak connectivity, while dual communities require a strong connectivity. This has significant consequences for supply networks such as power grids. Several approaches have been discussed to limit the connectivity of power grids to prevent the spreading of cascading failures. This includes concepts of microgrids⁴⁵ as well as intentional islanding⁴⁶ or tree-partitioning^{47,48}. However, future power grids will require more, not less connectivity to transmit renewable energy over large distances^{49,50}. Dual communities might resolve this conundrum, as they prevent failure spreading from one community to the other one, without limiting the network's ability to transmit energy. This is in stark contrast to primal communities that limit failure spreading from one community to the other one, but also supply. Thus, the construction of dual communities may also serve as a strategy against failure spreading, in line with other ideas brought forward recently³³.

Dual communities may be detected using the same techniques as for primal communities once the dual graph is constructed. We here focus on classical spectral methods based on the graph Laplacian, as this matrix naturally arises in the study of graph duality and linear flow networks. By now, numerous algorithms for community detection have been developed that outperform spectral methods depending on the respective application^{5,51,52}. All these algorithms can be readily applied to the dual graph. A short analysis for a selected example is provided in the Supplementary Information. One challenge remains for the generalization of this approach. For planar graphs, the dual is constructed by a straightforward geometric procedure. For non-planar graphs, a geometric analysis is much more involved⁵³. A dual can be constructed algebraically by choosing a basis of the cycle space. However, there is no distinguished basis such that the algebraic dual is not unique. The detailed analysis of community boundaries, in particular the inequality (Eq. (12)), may provide an alternative route to generalize the definition of network communities. For instance, one may choose a decomposition to minimize the dual topological connectivity μ_2^* .

Finally, we note that other approaches have been put forward to generalize the definition of network communities beyond the paradigm of strong mutual connectivity. For instance, communities can be defined in terms of the similarity of the connectivity of nodes (see, e.g., refs. 54, 55) or from spreading processes⁵⁶. The graph dual approach presented here emphasizes the role of the community boundaries, both in the definition of the community structure and in its impact on spreading processes and network robustness. Furthermore, graph duality provides a rigorous algebraic justification for our generalization of community structures.

Methods

Global cascade model

In Fig. 1, we show results from a classic model of global cascades. The state of each node $i = 1, \dots, N$ in time step t is denoted as $s_i(t) \in \{0, 1\}$, encoding healthy/operational and infected/faulty, respectively. A node becomes infected/faulty in time step $t + 1$ if the weighted average of the neighboring nodes exceeds a threshold ϕ_i :

$$s_i(t+1) = \begin{cases} 1 & \text{if } \frac{\sum_k w_{ik} s_k}{\sum_k w_{ik}} > \phi_i \\ 1 & \text{if } s_i(t) = 1 \\ 0 & \text{else.} \end{cases} \quad (22)$$

This model is iterated until no further changes of the node states occur.

We simulate this model on a square lattice with inhomogeneous edge weights. A fraction $p_e = 0.8$ of edges connecting the center nodes of the lattice with its nearest neighbors is selected at random. The weight of these edges is set to $w_{ij} = w_e$, where w_e is a tunable parameter, while all other edges have weight $w_{ij} = 1$. At time $t = 0$, we choose a fraction $\rho_0 = 0.05$ of all nodes in the left part and set them to state 1, while all other nodes are in state 0. For each value of the parameter w_e , we repeat the simulation for 1000 random initial conditions and record the fraction of nodes in state 1, denoted as ρ_∞ .

Creation of dual graphs: planar networks

In this manuscript, we mostly restrict our analysis to planar, connected graphs. A graph $G = (V, E)$ with vertex set V and edge set E is called planar if it may be drawn in the plane without two edges crossing⁵⁷. For a plane graph G , it is straightforward to establish a duality to another graph, referred to as the plane dual or simply dual graph and denoted as G^* . The dual graph is constructed using the cycles of graph G where a cycle is defined to be a path that starts and ends in the same vertex consisting of otherwise distinct vertices. For a graph with M edges and N nodes, these cycles form the graph's cycle space of dimension $N' = M - N + 1$. A particular basis of this space is given by the faces of the plane embedding, such that the dual graph $G^* = (V^*, E^*)$ has a vertex corresponding to each face. Two dual vertices v_1^* and v_2^* are connected by a dual edge $e^* = (v_1^*, v_2^*) \in E^*(G^*)$ if the two corresponding cycles share an edge. For a weighted graph, the edge weight of the dual edge is chosen to be the inverse of the corresponding edge shared by the two cycles. Furthermore, we adopt the following convention; if two cycles share k edges e_1, \dots, e_k with weights w_1, \dots, w_k , we lump them together into a single dual edge e^* with edge weight $w^* = \sum_{i=1}^k w_i^{-1}$ thus avoiding multi-edges in the dual graph and refer to this model as the reduced dual graph. Note that the definition of the edge-cycle incidence matrix C needs to be adjusted for the reduced dual graph.

Creation of dual graphs: non-planar networks

For non-planar networks, the basis of the cycle space may no longer be uniquely determined based on the graph's embedding. Different basis choices result in different dual graphs. When calculating the dual graph of the non-planar European topology shown in Fig. 5f–g, we used the graphs' minimum cycle basis to create the dual graph.

Hierarchical decomposition of dual graph

We assign m hierarchy levels based on repeated spectral bisection of the dual graph using the following procedure:

1. Assign dual communities to the graph by making use of the Fiedler vector \mathbf{v}_2^* of the dual graph G^*
2. Identify the edges that lie on the boundary between the two communities by checking for edges in the primal shared by faces corresponding to dual nodes of both communities

3. Remove the boundary edges from the graph thus creating two primal subgraphs G_1 and G_2
4. Repeat the process m times

Building supply networks with fluctuating sources

Our framework extends the fluctuating sink model proposed by Corson³⁶ where a single, fluctuating source supplies the remaining network. To this end, we consider a linear flow network with sources and sinks attached to the nodes and model the sinks as Gaussian random variables $P \in \mathcal{N}(\mu, \sigma)$. In contrast to previous work, we consider multiple sources, N_s in number, whose statistics can be derived from the statistics of the sinks due to the fact that the in- and outflows at the nodes need to sum to zero (see Supplementary Information). We then add additional fluctuations to the sources that are built using Dirichlet random variables $X_i \sim \text{Dir}(\alpha)$. The fluctuations are constructed such that they only influence the statistics of the sources and their variance is tuned by a single parameter α . To be able to tune the influence of this additive noise variable, we introduce a scale parameter $K \in \mathbb{R}$. The inflow at a source at a given point in time is then given by (see Supplementary Information)

$$P_{s_i} = -\frac{1}{N_s} \sum_{i=N_s+1}^N P_i + K \left(\frac{1}{N_s} - X_i \right), \quad (23)$$

where P_i are the outflows at the sinks. Here, we arranged the node order such that the sources have indices $1, \dots, N_s$ and sinks are numbered as $N_s + 1, \dots, N$. To produce Fig. 5, we considered a network with $N_s = 2$ and fix the parameters of the Gaussian distribution as $\mu = -1$, $\sigma = 0.1$. The scale parameter is set to $K = 500$ and the parameter α controlling the statistics of the Dirichlet distribution is varied in the interval $\alpha \in [10^{-2}, 10^4]$, thus changing the variance of the Dirichlet variables $\sigma_D^2 = K^2 \frac{(N_s-1)}{N_s^2(N_s\alpha+1)}$ (see Supplementary Information).

Analysis of power grid datasets

The networks shown in Fig. 5f, g were determined using the open energy system model 'PyPSA-Eur' cost-optimizing the generation infrastructure and operation as well as the transmission grid for different levels of carbon-dioxide emission reductions with respect to the emission levels in 1990. For each target carbon-dioxide emission reduction level, the network is optimized for an entire year with the weather conditions of 2013 and 3-hourly resolution (see ref. 39 for further details on the optimization model). To analyze the network topology, we set the weight w_ℓ of a line ℓ to the maximal apparent power that can flow through it. Note that this is different from weighting the line by its line susceptance and allows us to also incorporate high-voltage DC lines. To determine the level of fluctuating renewables shown in Fig. 5f, g, we calculate the share of the total annual generation in the entire system that is produced by fluctuating renewables. To this end, we assume that the following technologies are fluctuating renewable energy sources: offshore wind AC, offshore wind DC, onshore wind, run-of-the-river hydroelectricity (ror) and solar. In Supplementary Figs. S3 and S4 we show as an example the generation for two months and carbon emission reduction levels over time and on the network level.

Data availability

The topology of the Central European power grid have been extracted from the open European energy system model PyPSA-Eur³⁹, which is fully available online⁵⁸. Leaf data was provided by the authors of ref. 59 and is available from the respective authors upon request. The leaf venation networks are based on microscopic recordings. Edge conductivities w_{ij} are assumed to scale with the radius r_{ij} of the corresponding vein (i, j) as $w_{ij} \propto r_{ij}^4$ according to the Hagen-Poiseuille law (see ref. 60 for a detailed discussion). We used the radius in pixels at a

resolution of 6400 dpi. The data generated in this study (effective topology of power grid networks and selected leaf venation networks) as well as essential computer code for data processing have been deposited in a Zenodo repository⁶¹.

Code availability

Computer code is available on github⁶² with the specific version used in this publication being archived at Zenodo⁶¹.

References

1. Radicchi, F., Castellano, C., Cecconi, F., Loreto, V. & Parisi, D. Defining and identifying communities in networks. *Proc. Natl Acad. Sci. USA* **101**, 2658–2663 (2004).
2. Girvan, M. & Newman, M. E. J. Community structure in social and biological networks. *Proc. Natl Acad. Sci. USA* **99**, 7821–7826 (2002).
3. Fletcher, R. J. et al. Network modularity reveals critical scales for connectivity in ecology and evolution. *Nat. Commun.* **4**, 2572 (2013).
4. Shekhtman, L. M., Shai, S. & Havlin, S. Resilience of networks formed of interdependent modular networks. *N. J. Phys.* **17**, 123007 (2015).
5. Newman, M. E. J. Modularity and community structure in networks. *Proc. Natl Acad. Sci. USA* **103**, 8577–8582 (2006).
6. Newman, M. E. J. Communities, modules and large-scale structure in networks. *Nat. Phys.* **8**, 25–31 (2012).
7. Guimera, R. & Nunes Amaral, L. A. Functional cartography of complex metabolic networks. *Nature* **433**, 895–900 (2005).
8. Manik, D. et al. Network susceptibilities: theory and applications. *Phys. Rev. E* **95**, 012319 (2017).
9. May, R. M. Will a large complex system be stable? *Nature* **238**, 413 (1972).
10. Gilarranz, L. J., Rayfield, B., Liñán-Cembrano, G., Bascompte, J. & Gonzalez, A. Effects of network modularity on the spread of perturbation impact in experimental metapopulations. *Science* **357**, 199–201 (2017).
11. Katifori, E., Szöllösi, G. J. & Magnasco, M. O. Damage and fluctuations induce loops in optimal transport networks. *Phys. Rev. Lett.* **104**, 048704 (2010).
12. Gavrilchenko, T. & Katifori, E. Resilience in hierarchical fluid flow networks. *Phys. Rev. E* **99**, 012321 (2019).
13. Viana, M. P., Strano, E., Bordin, P. & Barthelemy, M. The simplicity of planar networks. *Sci. Rep.* **3**, 3495 (2013).
14. Barthelemy, M. Spatial networks. *Phys. Rep.* **499**, 1–101 (2011).
15. Barthelemy, M. *Morphogenesis of Spatial Networks* (Springer International Publishing, 2018).
16. Barthelemy, M. *The Structure and Dynamics of Cities: Urban Data Analysis and Theoretical Modeling* (Cambridge University Press, 2016).
17. Manik, D., Timme, M. & Witthaut, D. Cycle flows and multistability in oscillatory networks. *Chaos* **27**, 083123 (2017).
18. Dörfler, F., Chertkov, M. & Bullo, F. Synchronization in complex oscillator networks and smart grids. *Proc. Natl Acad. Sci. USA* **110**, 2005–2010 (2013).
19. Ronellenfitch, H., Timme, M. & Witthaut, D. A dual method for computing power transfer distribution factors. *IEEE Trans. Power Syst.* **32**, 1007–1015 (2017).
20. Ronellenfitch, H., Manik, D., Hörsch, J., Brown, T. & Witthaut, D. Dual theory of transmission line outages. *IEEE Trans. Power Syst.* **32**, 4060–4068 (2017).
21. Pourbeik, P., Kundur, P. & Taylor, C. The anatomy of a power grid blackout - root causes and dynamics of recent major blackouts. *IEEE Power Energy Mag.* **4**, 22–29 (2006).
22. Wood, A. J., Wollenberg, B. F. & Sheblé, G. B. *Power Generation, Operation and Control* (John Wiley & Sons, 2014).

23. Purchala, K., Meeus, L., Dommelen, D. V. & Belmans, R. Usefulness of DC power flow for active power flow analysis. In *IEEE Power Engineering Society General Meeting*, Vol. 1 454–459 (IEEE, 2005).
24. Watts, D. J. A simple model of global cascades on random networks. *Proc. Natl Acad. Sci. USA* **99**, 5766–5771 (2002).
25. Nematzadeh, A., Ferrara, E., Flammini, A. & Ahn, Y.-Y. Optimal network modularity for information diffusion. *Phys. Rev. Lett.* **113**, 088701 (2014).
26. Bollobás, B. *Modern Graph Theory*. No. 184 in *Graduate Texts in Mathematics* (Springer, 1998).
27. Dörfler, F., Simpson-Porco, J. W. & Bullo, F. Electrical networks and algebraic graph theory: models, properties, and applications. *Proc. IEEE* **106**, 977–1005 (2018).
28. Hwang, N. & Houghtalen, R. *Fundamentals of Hydraulic Engineering Systems* (Prentice Hall, 1996).
29. Díaz, S., González, J. & Minguez, R. Observability analysis in water transport networks: algebraic approach. *J. Water Resour. Planning Manag.* **142**, 04015071 (2016).
30. Fortunato, S. Community detection in graphs. *Phys. Rep.* **486**, 75–174 (2010).
31. European Network of Transmission System Operators for Electricity (ENTSO-E). Continental Europe synchronous area separation on 08 January 2021. ICS Investigation Expert Panel - final report. https://eepublicdownloads.azureedge.net/clean-documents/SOCdocuments/SOCReports/entso-e_CESysSep_Final_Report_210715.pdf (2021).
32. European Network of Transmission System Operators for Electricity (ENTSO-E). Outage of French-Spanish interconnection on 24 July 2021 - update. <https://www.entsoe.eu/news/2021/08/20/outage-of-french-spanish-interconnection-on-24-july-2021-update/> (2021).
33. Kaiser, F., Latora, V. & Witthaut, D. Network isolators inhibit failure spreading in complex networks. *Nat. Commun.* **12**, 3143 (2021).
34. Kaiser, F., Ronellenfisch, H. & Witthaut, D. Discontinuous transition to loop formation in optimal supply networks. *Nat. Commun.* **11**, 5796 (2020).
35. Fiedler, M. Algebraic connectivity of graphs. *Czechoslovak Math. J.* **23**, 298–305 (1973).
36. Corson, F. Fluctuations and redundancy in optimal transport networks. *Phys. Rev. Lett.* **104**, 048703 (2010).
37. Bohn, S. & Magnasco, M. O. Structure, scaling, and phase transition in the optimal transport network. *Phys. Rev. Lett.* **98**, 088702 (2007).
38. Dodds, P. S. Optimal form of branching supply and collection networks. *Phys. Rev. Lett.* **104**, 048702 (2010).
39. Hörsch, J., Hofmann, F., Schlachtberger, D. & Brown, T. PyPSA-eur: an open optimisation model of the european transmission system. *Energy Strategy Rev.* **22**, 207–215 (2018).
40. Guo, J., Fu, Y., Li, Z. & Shahidepour, M. Direct calculation of line outage distribution factors. *IEEE Trans. Power Syst.* **24**, 1633–1634 (2009).
41. Strake, J., Kaiser, F., Basiri, F., Ronellenfisch, H. & Witthaut, D. Non-local impact of link failures in linear flow networks. *N. J. Phys.* **21**, 053009 (2019).
42. Motter, A. E., Myers, S. A., Anghel, M. & Nishikawa, T. Spontaneous synchrony in power-grid networks. *Nat. Phys.* **9**, 191–197 (2013).
43. Dörfler, F. & Bullo, F. Synchronization in complex networks of phase oscillators: a survey. *Automatica* **50**, 1539–1564 (2014).
44. Acebrón, J. A., Bonilla, L. L., Vicente, C. J. P., Ritort, F. & Spigler, R. The kuramoto model: a simple paradigm for synchronization phenomena. *Rev. Mod. Phys.* **77**, 137 (2005).
45. Lasseter, R. H. Microgrids. In *2002 IEEE Power Engineering Society Winter Meeting Conference Proceedings (Cat. No. 02CH37309)*, Vol. 1 305–308 (IEEE, 2002).
46. Mureddu, M., Caldarelli, G., Damiano, A., Scala, A. & Meyer-Ortmann, H. Islanding the power grid on the transmission level: less connections for more security. *Sci. Rep.* **6**, 1–11 (2016).
47. Bialek, J. W. & Vahidinasab, V. Tree-partitioning as an emergency measure to contain cascading line failures. *IEEE Trans. Power Syst.* **37**, 467–475 (2021).
48. Zocca, A., Liang, C., Guo, L., Low, S. H. & Wierman, A. A spectral representation of power systems with applications to adaptive grid partitioning and cascading failure localization. Preprint at <https://arxiv.org/abs/2105.05234> (2021).
49. Schlachtberger, D. P., Brown, T., Schramm, S. & Greiner, M. The benefits of cooperation in a highly renewable european electricity network. *Energy* **134**, 469–481 (2017).
50. Tröndle, T., Lilliestam, J., Marelli, S. & Pfenninger, S. Trade-offs between geographic scale, cost, and infrastructure requirements for fully renewable electricity in europe. *Joule* **4**, 1929–1948 (2020).
51. Peixoto, T. P. Hierarchical block structures and high-resolution model selection in large networks. *Phys. Rev. X* **4**, 011047 (2014).
52. Ghasemian, A., Hosseinmardi, H. & Clauset, A. Evaluating overfit and underfit in models of network community structure. *IEEE Trans. Knowledge Data Eng.* **32**, 1722–1735 (2019).
53. Modes, C. D., Magnasco, M. O. & Katifori, E. Extracting hidden hierarchies in 3D distribution networks. *Phys. Rev. X* **6**, 031009 (2016).
54. Moore, C., Yan, X., Zhu, Y., Rouquier, J.-B. & Lane, T. Active learning for node classification in assortative and disassortative networks. In *Proceedings of the 17th ACM SIGKDD International Conference on Knowledge Discovery and Data Mining* 841–849 (ACM, 2011).
55. Garcia, J. O., Ashourvan, A., Muldoon, S., Vettel, J. M. & Bassett, D. S. Applications of community detection techniques to brain graphs: algorithmic considerations and implications for neural function. *Proc. IEEE* **106**, 846–867 (2018).
56. Schaub, M. T., Lehmann, J., Yaliraki, S. N. & Barahona, M. Structure of complex networks: quantifying edge-to-edge relations by failure-induced flow redistribution. *Netw. Sci.* **2**, 66–89 (2014).
57. Diestel, R. *Graph Theory* (Springer, 2000).
58. Hörsch, J., Neumann, F., Hofmann, F., Schlachtberger, D. & Brown, T. PyPSA-Eur: an open optimisation model of the european transmission system (Dataset). <https://doi.org/10.5281/zenodo.3886532> (2020).
59. Ronellenfisch, H., Lasser, J., Daly, D. C. & Katifori, E. Topological phenotypes constitute a new dimension in the phenotypic space of leaf venation networks. *PLOS Comput. Biol.* **11**, e1004680 (2015).
60. Coomes, D. A., Heathcote, S., Godfrey, E. R., Shepherd, J. J. & Sack, L. Scaling of xylem vessels and veins within the leaves of oak species. *Biol. Lett.* **4**, 302–306 (2008).
61. Böttcher, P. C. & Kaiser, F. Data and code accompanying “Dual communities in spatial networks”. <https://doi.org/10.5281/zenodo.7243770> (2022).
62. Böttcher, P. C. & Kaiser, F. Dual communities. <https://github.com/phboett/dual-communities> (2022).

Acknowledgements

We thank Torsten Eckstein for providing some of the digitized leaf networks, Tom Brown and Fabian Neumann for providing us with the optimized power grids, and Eleni Katifori for helpful discussions. We gratefully acknowledge support from the German Federal Ministry of Education and Research (BMBF) via the grant “CoNDyNet2” with grant no. 03EK3055B, the Helmholtz Association via the grant “Uncertainty Quantification – From Data to Reliable Knowledge (UQ)” with grant no. ZT-I-0029 and the Deutsche Forschungsgemeinschaft (DFG, German Research Foundation) with grant No. 491111487.

Author contributions

D.W. conceived research and acquired funding. F.K. and D.W. designed research. F.K. carried out all numerical simulations. F.K. and P.C.B. evaluated the results and designed the figures. All authors contributed to discussing the results and writing the manuscript.

Funding

Open Access funding enabled and organized by Projekt DEAL.

Competing interests

The authors declare no competing interests.

Additional information

Supplementary information The online version contains supplementary material available at <https://doi.org/10.1038/s41467-022-34939-6>.

Correspondence and requests for materials should be addressed to Dirk Witthaut.

Peer review information *Nature Communications* thanks Wenjun Mei, Talal Rahwan, and the other, anonymous, reviewer(s) for their contribution to the peer review of this work.

Reprints and permissions information is available at <http://www.nature.com/reprints>

Publisher's note Springer Nature remains neutral with regard to jurisdictional claims in published maps and institutional affiliations.

Open Access This article is licensed under a Creative Commons Attribution 4.0 International License, which permits use, sharing, adaptation, distribution and reproduction in any medium or format, as long as you give appropriate credit to the original author(s) and the source, provide a link to the Creative Commons license, and indicate if changes were made. The images or other third party material in this article are included in the article's Creative Commons license, unless indicated otherwise in a credit line to the material. If material is not included in the article's Creative Commons license and your intended use is not permitted by statutory regulation or exceeds the permitted use, you will need to obtain permission directly from the copyright holder. To view a copy of this license, visit <http://creativecommons.org/licenses/by/4.0/>.

© The Author(s) 2022